Cytokinin acts as a systemic signal coordinating reproductive effort in Arabidopsis

Darya Volkava[1,2], Sona Valuchova Bukovcakova[1], Pavlina Mikulkova[1], Jana Pecinkova[1], Jan Skalak[1], Jan Hejatko[1], Karel Riha[1]

[1]Central European Institute of Technology (CEITEC), Masaryk University, Brno, Czech Republic

[2]National Centre for Biomolecular Research, Faculty of Science, Masaryk University, Brno, Czech Republic

Correspondence: karel.riha@ceitec.muni.cz; darya.volkava@ceitec.muni.cz

Abstract

The duration of the flowering phase is a key adaptive trait related to reproductive effort and plant longevity. In plants with indeterminate inflorescences, the number of flowers produced is determined by the activity of the inflorescence meristem. However, the integration of inflorescence meristem activity with the physiological and developmental status of a plant is not well understood. We combined quantitative imaging of the inflorescence meristem with the manipulation of cytokinin levels and distribution to investigate how meristem activity is regulated. Our data support the hypothesis that emerging fruits drain the acropetal flow of cytokinin away from the meristem inducing its proliferative arrest. We further show that the duration of flowering and cytokinin signaling in the inflorescence meristem is influenced by nitrate availability. Taken together, these data suggest that cytokinin functions as a systemic signal that integrates information about ongoing reproductive effort and plant nutrient status to control flower production.

Introduction

In contrast to animals, plants exhibit a remarkable flexibility in their body structure, continuously generating new organs and tissues through post-embryonic growth. This developmental plasticity allows plants to dynamically adapt their physical structure to local environmental conditions and adjust their life strategy accordingly (1). Central to this process is flower production, a key developmental trait that is directly related to reproductive effort. The timing and duration of the flowering phase determine seed yield, quality, and reproductive success. However, allocating resources to fruit and seed production is an energetically demanding task, so deciding how many flowers to produce must be integrated with developmental and environmental cues (2, 3).

In plants with indeterminate inflorescences, the number of flowers is limited by proliferative arrest (PA) of the inflorescence meristem, which occurs after production of a certain number of fruits. A major factor controlling the arrest is seed production, since surgical removal of fruits or mutations causing infertility greatly extend the activity of the inflorescence meristem and the life span of the plant (4-7). Two hypotheses have been proposed to explain the corelative control of flower formation by developing seeds (8-10). The "death hormone" hypothesis predicts the existence of a factor produced by the fruit or seed that is transported to other tissues where it induces the cessation of growth. The "nutrient drain" hypothesis suggests that developing reproductive organs represent a strong sink that diverts resources or signaling molecules that sustain growth away from vegetative tissues.

The corelative inhibition between reproductive organs of the same plant was described in a number of species, but deeper insights into this phenomenon have been obtained only recently by studies in *Arabidopsis thaliana* (10-12). The primary inflorescence in Arabidopsis becomes inactive after production of ~30-50 flowers and arrests with a cluster of unopened floral buds (6, 13). The cessation of flower development occurs in two steps. The inflorescence meristem stops initiating new flower primordia 2-3 weeks after bolting, which is followed by the full arrest of floral bud development several days later (14, 15). Transcriptomic analysis revealed that the arrested meristem and floral buds enter a dormancy-like state that can be reverted into an active state by fruit removal in a process that resembles release of axillary buds from apical dominance (16).

Several molecular pathways have been implicated in the inflorescence arrest. As the plant ages, the inflorescence meristem gradually diminishes in size, which is accompanied by the downregulation of the stem cell maintenance factor WUSCHEL (WUS) (14, 16-19). The age-dependent decline of WUS involves

52 FRUITFUL/APETALA2 regulatory module (18, 20), but its coordination with reproductive processes
53 remains unknown. Jasmonic and abscisic acid signaling also contributes to establishment of proliferative
54 arrest and disruption of these signaling pathways extends the flower production (21, 22). The onset of
55 floral arrest is highly susceptible to fruit formation in the vicinity of the inflorescence meristem (23). It has
56 been proposed that the fruits proximal to the inflorescent meristem exert an inhibitory effect via auxin
57 canalization. According to this model, increasing auxin flow from emerging fruits disrupts the polar auxin
58 transport from inflorescence apex causing its arrest (14, 23).

59 However, the inhibitory effect of fruits on inflorescence apex becomes effective only when the meristem
60 reaches a certain age and develops competence for arrest (23). This indicates existence of an additional
61 mechanism that tracks the reproductive and developmental age of the meristem. Recent studies have
62 shown downregulation of cytokinin signaling during inflorescence arrest, and that exogenous application
63 of cytokinin to the inflorescence meristem delays or even reverts the arrest (15, 19). Furthermore,
64 mutations in genes involved in cytokinin signaling significantly affect inflorescence arrest (15, 20, 24-27).
65 In shoot apical meristem, cytokinin reinforces expression of WUS in a positive feedback loop and helps to
66 maintain the undifferentiated state of stem cells (28). In addition, cytokinin stimulates cell proliferation
67 and meristematic activity by promoting CYCLIN D expression (29). Thus, it is likely that cytokinin signaling
68 plays a central role in regulating inflorescence arrest.

69 Cytokinins act as long-distance signaling molecules and some of their forms are produced in roots and
70 transported via xylem into shoot to regulate growth and developmental processes (30, 31). Developing
71 seeds and embryos exhibit high level of cytokinin, and at least part of it may be provided from maternal
72 plant (32). Thus, the emerging fruits with developing seeds may represent a sink that diverts cytokinin
73 transport from the inflorescence apex, leading to decline in cytokinin signaling in the inflorescence
74 meristem and increasing its competence to proliferative arrest. In this study we used quantitative imaging
75 to investigate whether cytokinin acts as a systemic signal that integrates physiological and developmental
76 cues to coordinate flower production and reproductive efforts.

77 **Results**

78 ***Meristems become permissible to inflorescence arrest at older age***

79 Under our experimental conditions, *A. thaliana* Col-0 produces in average 53 flowers on the primary
80 inflorescence (PI) in about 25 days before proliferative arrest occurs (Supplementary Fig. 1). Continuous
81 pruning of flowers on the PI substantially increased both the number of flowers and the duration of the

82 flower production. The first 30 flowers have a negligible effect on the onset of inflorescence arrest and
83 their removal did not significantly alter the duration of flowering or the number of flowers produced.
84 However, continuous pruning of flowers appearing after the development of the first 30 flowers had the
85 same impact as removing all flowers (Supplementary Fig. 1). These observations confirm the data of Ware
86 et al. (23) and suggest that the inflorescence arrest is primarily influenced by the production of apex-
87 proximal fruits and that it occurs only when the inflorescence meristem has passed a certain
88 developmental age and becomes susceptible to the arrest.

89 ***Quantitative imaging of inflorescence meristem***

90 The observation of diminished cytokinin signaling in the arrested meristem (15, 19) raised the question of
91 whether the declining transport of cytokinin to the inflorescence apex due to sink in developing fruits
92 determines the susceptibility of the meristem to arrest. Such scenario predicts that cytokinin signaling in
93 the meristem gradually decreases with the growth of new fruits. To test this hypothesis, we developed a
94 methodology for three-dimensional (3D) quantitative imaging of fluorescent reporters in inflorescence
95 meristems (IM) using light-sheet fluorescence microscopy (LSFM). In a standard confocal microscopy, the
96 apical meristem is scanned from the apex to the base, and scanning of a complete confocal stack in
97 multiple channels can take tens of minutes (33, 34). During image acquisition, the entire volume of the
98 meristem is illuminated by the excitation laser, which can partially quench the signal, leading to
99 inaccuracies in the signal quantification, especially in the deeper layers of the tissue.

100 LSFM allows fast 3D imaging of relatively macroscopic objects by passing them through a thin laser sheet,
101 which minimizes the photodamage. To accurately capture the 3D architecture and to minimize the effect
102 of 3D scanning on signal intensity in different layers, we imaged the inflorescence meristem laterally along
103 the axis of vertical symmetry from eight different angles (Fig. 1a). The resulting stacks were combined to
104 build a comprehensive 3D model of the inflorescence meristem (Supplementary Fig. 2, Fig. 1b, Movies 1
105 and 2). The intensity of each voxel in the model represents the average of the data obtained in the eight
106 scans. We used two different approaches for data analysis (Supplementary Fig. 2). For the *pCLV3::H2B-*
107 *mCherry* marker that gives a strong and well defined nuclear signal, we performed spot-based
108 segmentation and included the mean intensity of the signal from all detected nuclei in the meristem for
109 the downstream analyses (Fig. 1c-f). This provided an estimate of the size of the stem cell niche and the
110 intensity of the CLV3 expression.

111 The nuclear signal from *pWUS::WUS-linker-GFP* marker is weaker and more diffused compared to the
112 signal from *pCLV3::H2B-mCherry*, and the *pTCSn::GFP* and *DR5rev::GFP* markers are cytoplasmic,
113 rendering them unsuitable for spot-based segmentation. Therefore, the 3D models with these reporters
114 were segmented into individual cells using FM4-64-stained membranes, and the mean intensity of the
115 signal was calculated for each segmented cell. The decreasing size of the inflorescence meristem with
116 developmental age (17, 19) poses a challenge for the comparative analysis of meristems at different ages.
117 To overcome this issue, we focused on cells within the central zone of the meristem. The central zone of
118 Arabidopsis shoot apical meristem has been defined as cells within a 30 µm perimeter from its center (35).
119 To analyze comparable subsets of cells in the central zone, we focused on cells located within 21 µm radius
120 of the meristem apex (Fig. 1g-j). We observed that this volume still excludes areas where emerging flower
121 primordia start to protrude, even in the smallest arrested meristems. When comparing arrested
122 meristems to those two weeks after bolting (2 wab), we observed that cells in arrested meristems are
123 marginally smaller, resulting in a slightly higher cell count within the analyzed volume (Supplementary Fig.
124 3). However, this difference is negligible. Thus, the volume-based subset approach can be employed to
125 facilitate the quantitative analysis of the same group of cells within each meristem, ensuring comparability
126 of the data across different meristems.

127 ***Age-dependent changes in inflorescence meristem***

128 To assess the age-dependent changes in the inflorescence meristem, we quantified the expression of the
129 stem cell marker *pCLV3::H2B-mCherry* in inflorescence meristems (IM) from 1 day after bolting (dab) until
130 PA (Fig. 2a-e,u). Approximately 150-200 cells expressed *pCLV3::H2B-mCherry* in meristems from 1 dab to
131 2 wab, but the number decreased to less than 50 in the arrested meristem, consistent with its reduced
132 size (Supplementary Fig. 4a). We also observed differences in the signal intensity between meristems of
133 different ages. At 1 dab, *pCLV3::H2B-mCherry* expression was detected in a large area of the shoot apex
134 with less variation in signal intensity between detected nuclei (Fig. 2a). This is the time when the
135 inflorescence bolt is growing rapidly, but flowers have not yet opened. At 1 wab when the first flowers
136 began to open, *pCLV3::H2B-mCherry* expression was strongest in the middle of the central zone and
137 gradually decreased toward the peripheral zone (Fig. 2b). The signal intensity in the central zone further
138 increased and reached a maximum at 2 wab (Fig. 2c). At PA, the *pCLV3::H2B-mCherry* was restricted to a
139 small area of the central zone and signal intensity slightly decreased to levels comparable to meristems at
140 1 wab (Fig. 2d,u). This indicates that the stem cell niche is maintained at PA, although its size is significantly
141 reduced.

142 We next analyzed the stem cell maintenance factor WUS using the *pWUS::WUS-linker-GFP* reporter.
143 Expression of the WUS reporter was restricted to the deeper layers of the IM with the strongest signal at
144 1 dab, then its level decreased at 1 wab, and became undetectable at 2 wab (Fig. 2f-j,v). A similar pattern
145 was also observed with the cytokinin signaling reporter *pTCSn::GFP*, which was more strongly expressed
146 in the deeper cell layers compared to the uppermost layers (Supplementary Fig. 4d-f). The overall
147 *pTCSn::GFP* signal, highest at 1 dap, gradually declined and became nearly undetectable by 2 wab; no
148 signal was detected at PA (Fig. 2k-o,w). These data suggest that WUS expression and cytokinin signaling
149 do not decrease just before PA, but start to decline already from early stages of inflorescence bolt
150 formation.

151 Since inflorescence arrest was proposed to be caused by auxin (14, 23), we analyzed auxin signaling using
152 *DR5rev::GFP* sensor. Reporter expression was primarily restricted to the L1 layer, with local maxima
153 marking the initiation of floral primordia (Fig. 2p-t,x). Auxin signaling was high at 1 dab, its level peaked at
154 1 wab and then gradually declined reaching minima at PA. Nevertheless, even during PA, the *DR5rev::GFP*
155 signal was detectable at the putative initiation sites of floral primordia (Supplementary Fig. 4b,c). These
156 data show that PA is accompanied by a decrease in auxin signaling, which is preceded by a dampening of
157 cytokinin signaling. These observations are consistent with the idea that emerging fruits gradually divert
158 cytokinin transport from the IM, eventually rendering it susceptible to PA.

159 ***Fruit removal rapidly re-establishes cytokinin signaling in arrested meristem***

160 Removal of fruits reactivates the arrested meristem and restores cytokinin signaling and WUS expression
161 (Fig. 2j,o,v,w). Removal of competing sink organs may restore the acropetal flow of cytokinin into the IM
162 leading to its activation. Such an abrupt redirection of the cytokinin flow should result in a rapid
163 resumption of cytokinin signaling in the IM. Indeed, we observed statistically significant increase in the
164 *pTCSn::GFP* signal as early as two hours after pruning (hap), and the signal was very prominent at 6 hap
165 (Fig. 3a-e). In roots, the *pTCSn::GFP* reporter senses cytokinin with a delay of 30-60 min after exogenous
166 application of benzyl-aminopurine (Supplementary Fig. 5), suggesting that the level of cytokinin in the IM
167 starts to increase 1-1.5 h after the fruit removal.

168 IM reactivation leads to the resumption of the cell cycle, which can be monitored by the entry of cells into
169 S-phase. To examine the timing of this process, we visualized the *PCNA:TagRFP* reporter, which is
170 expressed in nuclei of proliferating cells and forms prominent nuclear speckles during S-phase (36, 37).
171 While numerous S-phase nuclei were readily detected in the IM 1 dab, no such nuclei were visible during

172 PA (Fig. 3f). Furthermore, the overall PCNA signal was low during PA, indicating a quiescent state of the
173 meristematic cells. First S-phase nuclei were detected 18 hap in floral buds and 24 hap in IM indicating
174 that floral buds resume growth before the IM.

175 ***Absence of fruits keeps inflorescence meristems physiologically younger***

176 Fruit production is a key determinant of longevity in many annual plants (4-7). In Arabidopsis, continuous
177 removal of fruits by pruning or infertility caused by a mutation substantially delay the onset of
178 proliferation arrest, extending the longevity of the IM and increasing flower production (Fig. 4a,b)(6). To
179 assess how the absence of seeds affects inflorescence meristem physiology, we analyzed CLV3 expression
180 along with auxin and cytokinin signaling in continuously pruned plants 2 wab. While inflorescence
181 meristems of both pruned and untreated plants showed a similar number of CLV3 positive stem cells, the
182 signal intensity was slightly lower in pruned plants (Fig. 4c-e). In contrast, auxin and cytokinin signaling
183 were significantly increased by pruning 2 wab (Fig. 4f-k), with signals comparable to untreated meristems
184 1 wab (Figure 2w,x). These data suggest that inflorescence meristems in seedless plants are in a
185 physiologically younger state than the age-matched meristems in fertile plants.

186 ***Manipulation of cytokinin levels in bolting plants affects the onset of PA***

187 The quantitative imaging data (Figs. 2w; 3e, 4i) show a strong anticorrelation between seed formation and
188 cytokinin signaling in the IM, indicating a causative role of cytokinin in linking reproductive effort to PA.
189 This is supported by the observations that mutants with aberrant cytokinin signaling show pronounced
190 changes in the onset of inflorescence arrest (15, 20, 25, 26). However, these mutants display pleotropic
191 vegetative growth phenotypes, which complicates the interpretation of the observed effects on the flower
192 production. To overcome this issue, we used an inducible system to modulate the cytokinin levels in adult
193 plants. We took advantage of plants expressing either CYTOKININ OXIDASE 2 from barley, which
194 deactivates cytokinin, (*proCaMV35S>GR>HvCKX2*), or bacterial ISOPENTENYL TRANSFERASE, which
195 mediates its biosynthesis (*proCaMV35S>GR>ipt*), from the dexamethasone (DEX) inducible promoter (38).
196 Transgene expression in these plants was induced by application of DEX solution to roots at different
197 stages of bolting. Induction of *proCaMV35S>GR>ipt* resulted in prolonged flowering and differentiation of
198 more flowers (Fig. 5a,b). In contrast, induction of *proCaMV35S>GR>HvCKX2* accelerated the inflorescence
199 arrest and reduced flower formation, with the earlier DEX application having the greater effect (Fig. 5c,d).

200 To further test whether local cytokinin deprivation in the IM impacts the PA, we sprayed the apex of the
201 main inflorescence bolt of *proCaMV35S>GR>HvCKX2* plants with DEX at 1 day after bolting and monitored

202 flower and fruit production until PA. The local DEX treatment abolished seed formation in subsequently
203 formed siliques (Fig. 5e), supporting the notion that cytokinin is required for placental activity and ovule
204 development (24). Fertility on the main inflorescence bolt was restored only in later-developed flowers
205 (Fig. 5e). Notably, despite the reduced seed set, PA occurred earlier in DEX treated plants compared to
206 mock-treated controls (Fig. 5f). This observation indicates that local cytokinin deprivation in shoot apex
207 overrides the effect of infertility on PA.

208 ***Role of cytokinin transport in fruit development and inflorescence arrest***

209 This experiment strongly supports the idea that cytokinin represents a systemic signal that regulates the
210 activity of IM. Cytokinins are primarily produced in roots and distributed via xylem to aboveground tissues
211 (30, 31). To test whether cytokinin can be transported shootwardly into the IM, we applied trans-Zeatin
212 (tZ) in lanolin to the internode between 20th and 21st fruit on the primary bolt during PA. This led to the
213 induction of *TCSn::GFP* signal in arrested IM and surrounding floral buds 48 hours after the treatment (Fig.
214 6a-d).

215 We next asked whether cytokinin is also transported into emerging fruits. Developing seeds are among
216 the tissues with the highest cytokinin levels, and cytokinins are key regulators of the seed size and number
217 (32, 39, 40). While it is well established that cytokinin biosynthesis occurs in developing seeds, the
218 contribution of transport from maternal tissues has been less explored (32). To address this question, we
219 analyzed plants deficient in cytokinin long-distance transport mediated by ATP-binding cassette
220 transporter subfamily G14 (ABCG14) (41, 42). Arabidopsis *abcg14* mutants have severely impaired root-
221 to-shoot translocation of tZ-type cytokinins and exhibit aberrant growth (41, 42) (Fig. 6e). We also found
222 that the number of fruits on PI was significantly reduced in *abcg14* compared to wild type, while the
223 duration of flowering was unaffected (Fig. 6f,g). This can be attributed to an increased plastochron ratio,
224 as also reported for mutants with impaired cytokinin production (43). In addition, consistent with the role
225 of cytokinin in regulating placental activity (24), *abcg14* mutants showed a reduced number of ovules and
226 mature seeds (Fig. 6h-j). Examination of cytokinin signalling using *TCSn::GFP* showed a very strong signal
227 in developing ovules and embryos in both wild type and *abcg14* plants (Fig. 6k-p), reaffirming that local
228 cytokinin biosynthesis occurs from the earliest stages of female reproductive development. Nevertheless,
229 *TCSn::GFP* was also observed in the replum and placenta during ovule development in wild type, but not
230 in *abcg14* mutants (Fig. 6k-p). These results suggest that ABCG14 mediates cytokinin transport into fruits
231 and that this process contributes to the seed formation.

232 We next analysed the reactivation of arrested IM in *abcg14* mutants. While fruit removal readily induced
233 the formation of fertile flowers in the wild type, less than 50% of *abcg14* mutants showed any signs of IM
234 reactivation 2 wap (Fig. 6q-s). Furthermore, the reactivated *abcg14* meristems rarely develop over 2 fertile
235 siliques. We also observed that *abcg14* mutants exhibit substantially reduced *TCSn::GFP* expression in the
236 inflorescence apex (Fig 6t,u) showing that ABCG14 is critical for cytokinin transport into shoot apex.
237 These data support the idea that reactivation of arrested IMs following fruit removal is mediated by the
238 redirection of ABCG14-meidated cytokinin transport to IM.

239

240 ***Nitrate availability modulates the onset of inflorescence arrest***

241 Flower formation and subsequent reproductive effort must be carefully coordinated with mineral nutrient
242 availability of to ensure successful reproduction and resource allocation. Cytokinins act as signaling
243 molecules that coordinate growth and developmental responses to nitrate availability (43, 44). To test
244 whether nitrate levels affect proliferative arrest and flower production, we grew plants on sand and
245 watered them with nutrient solution containing 5 mM KNO3 as the sole source of nitrogen. After bolting,
246 plants were treated with nutrient solution containing different concentrations of KNO3 (0, 2.5, 5, 7,5 or
247 10 mM) until PA (Fig. 7a). We observed a dose-dependent response to nitrate concentration in the
248 duration of flower production (Fig. 7b,c). We also observed a similar response in the number of rosette
249 inflorescences that were initiated after bolting (Fig. 7d). Unlike primary and rosette inflorescences, the
250 number cauline inflorescences (CI) was not affected (Fig. 7e) suggesting that nitrate-starved plants
251 preferentially release axillary buds on already developed inflorescences, rather than in the rosette.

252 To validate that these growth responses are related to changes in cytokinin signaling, we examined
253 *TCSn::GFP* expression in inflorescence meristems of plants supplemented with nutrient solution
254 containing 0, 5 or 10 mM KNO3 for two weeks after bolting (Fig. 7f-j). Plants deprived of nitrate (0 mM
255 KNO3) showed no *TCSn::GFP* expression in the IM, whereas an increasing signal was observed in
256 meristems watered with increasing concentrations of KNO3. These data suggest that the duration of
257 reproductive growth is modulated by nitrate availability using root-derived cytokinin as a long-distance
258 messenger.

259 **Discussion**

260 Reproduction is a resource-demanding process that in plants is supported by massive relocation of
261 nutrients from vegetative tissues, often leading to leaf senescence and demise of an entire organism (45,

262 46). Therefore, the ability to precisely coordinate the timing and duration of reproduction with
263 developmental and environmental cues is central to the evolutionary success of a species. In some plants,
264 the duration of flowering is determined by the activity of the inflorescence meristem, which is subject to
265 feedback control from seeds already produced. Such regulation must integrate information about ongoing
266 fruit and seed production, as well as nutrient availability and overall plant physiology. Recent studies in
267 Arabidopsis suggest that plant reproductive effort is monitored by auxin flux from newly emerging fruits
268 (14, 23). This process reduces auxin canalization from the adjacent developing floral buds, inducing their
269 growth arrest and dormancy.

270 Several studies have indicated a role of cytokinin in regulating inflorescence arrest and flower production
271 (15, 19, 20, 24-27). Here we provide evidence that cytokinin functions as a systemic signal that determines
272 the physiological status and proliferative capacity of the inflorescence meristem by integrating
273 information on reproductive effort and nutrient availability. We suggest that in line with the "nutrient
274 drain" hypothesis, the partitioning of shootwardly transported cytokinin into developing fruits reduces its
275 flux to the inflorescence meristem and ultimately induces the cessation of its activity.

276 Several lines of evidence support this scenario. First, our data from *abcg14* mutants indicate that
277 developing fruits act as a sink for cytokinin transport (Fig. 6k-p). Second, cytokinin signalling in the IM
278 gradually declines as new fruits are formed (Fig. 2), and this process is delayed by continuous fruit removal
279 (Fig. 4). Third, reactivation of an arrested meristem by pruning is accompanied by a rapid activation of
280 cytokinin signalling, possibly due to the redirection of cytokinin transport caused by the removal of
281 competing sinks (Fig. 3). This is further substantiated by the observation that cytokinin transport mutants
282 are impaired in meristem reactivation (Fig. 6q-u). Finally, manipulation of cytokinin levels through
283 inducible deactivation or biosynthesis during bolting has a pronounced effect on the onset of meristem
284 arrest (Fig. 5). Importantly, local cytokinin deactivation mitigates the effect of reduced fertility on
285 proliferation arrest, providing a strong support to the idea that cytokinin flow represents the mechanism
286 linking plant reproductive status with meristem activity.

287 The timing of inflorescence arrest and flower production are also affected by other physiological
288 parameters, such as carbohydrate status, photo-thermal conditions and nitrate concentration (Fig. 7) (14,
289 47). Cytokinin regulates growth responses to nitrate (43, 44) and thus may also integrate inputs on
290 nutrient availability to fine-tune plant reproductive effort.

291 The correlative inhibition of plant growth by fruits and seeds is a well-documented phenomenon with
292 significant practical implications, observed in numerous plants (11). Two alternative scenarios, known as
293 the "death hormone" and "nutrient drain" hypotheses, have been proposed to explain these observations.
294 These scenarios are not necessarily mutually exclusive. Auxin may function as a "death hormone" by being
295 canalized basipetally from developing seeds, providing information about fruit production near the
296 inflorescence meristem. Conversely, shootwardly-mobile cytokinin may serve as a more systemic signal
297 that is "drained" by newly emerging sink organs, thus providing a broader perspective on plant
298 physiological status and reproductive effort. Together, these mechanisms suggest a complex interplay of
299 hormonal signaling that coordinates growth and reproduction in plants, allowing adaptive responses to
300 changing environmental and developmental conditions.

301 **Methods**

302 ***Plant material and growth conditions***

303 All plants used in the study were *Arabidopsis thaliana* ecotype Col-0, with the exception of the *abcg14*
304 mutant which is in the Col-4 background. Plants were grown in a growth chamber at 21°C with 50-60%
305 humidity under 16h/8h light/dark cycles (light intensity 150 µmol m^{-2} s^{-1}) in a 3:1 by volume mixture of
306 soil:vermiculite. The following Arabidopsis lines were used in the study: *pCLV3::H2B-mCherry* (48),
307 *pWUS::WUS-linker-GFP* (49), *DR5rev::GFP* (50), *TCSn::GFP* (51), *PCNA:TagRFP* (36),
308 *proCaMV35S>GR>HvCKX2* (52), *proCaMV35S>GR>ipt* (38), and *abcg14* (41). In the original *pWUS::WUS-*
309 *linker-GFP* line, the construct complemented vegetative defect of *wus* mutant (GABI-Kat line GK870H12)
310 phenotype, but plants were semi-sterile. Because sterility and semi-sterility affects flower production, we
311 outcrossed the *wus* mutation and the resulting line in wild type background, which did not show any
312 growth or fertility defects, was analyzed.
313

314 ***Plant treatments***

315 The *proCaMV35S>GR>HvCKX2* and *proCaMV35S>GR>ipt* plants were induced at the indicated time points
316 by watering each plant with 50 ml of 10 µM dexamethasone. Control plants were watered with 50 mL of
317 0.0001 % (v/v) DMSO. For local treatment, plants were induced by direct application of 10 µl of 10 µM
318 dexamethasone to inflorescence at 1 dab; control plants were treated with 0.0001 % (v/v) DMSO. For
319 cytokinin application to the inflorescence bolt, trans-zeatin (10 mM in DMSO) was mixed with lanolin
320 paste at a ratio of 3:100 (v/v) and the paste was applied to the internode between fruits 20 and 21 counted

321 from the top cluster of arrested buds. For the nitrate resupply experiment, seedlings were germinated on
322 soil for 7 days, transferred to individual pots with the sand/zeolite mixture in the ratio 3:2 (v/v) pre-
323 watered with 50 mL of nutrient solution (53) containing 5 mM KNO3, 2 mM MgSO4, 3 mM CaCl2, 2.5 mM
324 KH2PO4 (adjusted to pH 5.5), 70 µM H3BO3, 14 µM MnCl2, 0.5 µM CuSO4, 1 µM ZnSO4, 0.2 µM NaMoO4,
325 10 µM NaCl, 0.01 µM CoCl2, 50 µM Fe-EDTA. Plants were fed with 25 mL of the nutrient solution weekly
326 until bolting. From bolting, plants were watered weekly with 50 mL of the nutrient solution supplemented
327 with either 5 mM KCl (0 mM NO3), or 2.5 mM KNO3, 2.5 mM KCl (2.5 mM NO3), or 5 mM KNO3 (5 mM
328 NO3), or 7.5 mM KNO3 (7.5 mM NO3), or 10 mM KNO3 (10 mM NO3).

329 ***Phenotyping of reproductive growth***

330 We used nomenclature as in Ware et al. (23): primary inflorescence is produced by the primary embryonic
331 shoot apex; secondary inflorescences are formed from axillary buds in the axils of cauline leaves (cauline
332 inflorescence) and rosette leaves (rosette inflorescence). For the developmental timing data plants were
333 assessed daily for beginning of bolting (scored upon appearance of visually detectible primary
334 inflorescence from leaves rosette) and inflorescence arrest (scored when there are no more open flowers
335 on inflorescence). The number of fruits and inflorescences was recorded after PA unless stated otherwise.
336 Reproductive growth of inflorescence was defined as the period from the beginning of bolting to PA.
337

338 ***Inflorescence meristem imaging***

339 The inflorescence meristem was dissected with sharp tweezers under a stereomicroscope in a drop of ½
340 MS medium supplemented with sucrose (5%); all pedicels with flower buds were carefully removed. For
341 plasma membrane staining, a drop of fresh FM™4-64 dye (Invitrogen, ref. number T13320; concentration
342 0.1 mg/mL) was applied to a glass slide and the tissue was stained for 2 min. Without prior washing, the
343 IM was inserted into a glass capillary (Brand: size 4, blue, ref. number 701910) filled with cooled but liquid
344 mounting medium (½ MS 5 % sucrose with 1% low melting agarose) containing well vortexed fluorescent
345 beads (1 µl of beads per 200 µl of the media; Invitrogen, FluoSpheres™ polysterene, size 1 µm; red
346 (580/605) ref. number F13083; blue/green (430/465) ref. number F13080), and the medium was solidified
347 for 5 min. Microscopy was performed with a Light-sheet Z.1 microscope (Zeiss). The capillary was inserted
348 into the microscope chamber containing liquid 5xMS medium (36) and the sample was slightly pushed out
349 of the capillary into liquid medium of the chamber. Imaging was performed using 20x objectives
350 (Detection optics 20x/1.0), dual side illumination (illumination optics 10x/0.2) and two-track imaging with
351 488 nm laser for GFP/YFP, and 561 nm laser for TagRFP/mCherry/FM4-64.

352

353 ***Image processing***

354 Raw data in .czi format were deconvolved in ZEN (Zeiss) using the regularized inverse filter, strength 2.
355 During this step, images form dual side illumination were fused to a single image. Deconvolved .czi files
356 were imported into FIJI and using the Multiview reconstruction plugin (54) Z stacks from all 8 angles were
357 registered and aligned using the fluorescent bead signal (Fast descriptor-based, translation invariant
358 model to regularize with affine). The same registration was then applied to the second channel, which did
359 not contain the fluorescent bead signal from. All angles were then fused together and exported in .ics/.ids
360 format. Using the Imaris file converter (ImarisFileConverter 9.2.1), the fused image was converted to .ims
361 format and opened in the Imaris software (Imaris 9.2.1). Segmentation was performed based on signal
362 localization. For the cytoplasmic signal, the segmentation algorithm "cells" was selected and using the
363 wizard, membranes were selected for segmentation (cell smallest diameter 2.5 µm, automatic cell
364 membrane threshold). The surface was generated from segmented cells. A reference frame was then
365 manually positioned at the apex and a filter for 21µm distance from the reference frame was then applied
366 to the surfaces. Signal artifacts present outside of the meristem were manually curated. The pixel intensity
367 mean from the channel containing the cytoplasmic signal was then exported from the clean filtered
368 selection. For the *pCLV3::H2B-mCherry* nuclear signal, the segmentation algorithm "spots" was selected
369 and 2 µm spheres were detected directly in the analysed channel. Due to the low experimental
370 background, all spots with the threshold 0 were included and therefore no filtering was necessary, as we
371 were confident that they all belonged to meristematic tissue. Values of pixel intensity mean from all spots
372 were exported. Fluorescence intensity of *TCSn::GFP* expression in roots was measured as described (55).

373 ***Data analysis***

374 For each meristem, values of the mean signal intensity for each segmented cell/spot (hereafter "data
375 point") and the distance of the data point from a reference frame in x-y-z were exported (Supplemental
376 Tables 1-5), and analyzed by statistical tests specified in the figure legends using R. For each age group or
377 treatment condition, 5 inflorescence meristems were imaged and their data points were pooled for
378 analysis (Supplemental Table 6). Signal intensity was plotted in R using ggplot2
379 (https://doi.org/10.1007/978-3-319-24277-4_9). 3D scatter plots representing models of individual IMs
380 analyzed in this study are provided in the Supplemental Data Set. These 3D plots were generated using
381 Plotly (https://github.com/plotly/plotly.R).

Acknowledgements

This work was funded by the Czech Science Foundation (23-07969X) and by the Ministry of Education, Youth, and Sports of the Czech Republic from the project TowArds Next GENeration Crops, reg. no. CZ.02.01.01/00/22_008/0004581 of the ERDF Programme Johannes Amos Comenius. We acknowledge the support from CEITEC MU Core facilities Plant Sciences and CELLIM, supported by the Czech-Bioimaging (No. LM2018129) infrastructure project funded by MEYS CZ. We also thank Dr. Ortrun Mittelsten Scheid, Dr. Jan Lohmann and Dr. Helene Robert Boisivon for providing reporter lines used in this study. Finally, we are indebted to Dr. Tom Bennett and Dr. Vivek Raxwal for their valuable comments and discussion on this paper.

Literature

1. S. E. Sultan, Phenotypic plasticity for plant development, function and life history. *Trends Plant Sci* **5**, 537-542 (2000).
2. Y. Y. Yang, J. G. Kim, The optimal balance between sexual and asexual reproduction in variable environments: a systematic review. *Journal of Ecology and Environment* **40**, 12 (2016).
3. K. G. S. Dani, U. Kodandaramaiah, Plant and Animal Reproductive Strategies: Lessons from Offspring Size and Number Tradeoffs. *Frontiers in Ecology and Evolution* **5** (2017).
4. S. J. Lindoo, L. D. Nooden, The Interrelation of Fruit Development and Leaf Senescence in 'Anoka' Soybeans. *Botanical Gazette* **137**, 218-223 (1976).
5. J. E. Dale, Some Effects of the Continuous Removal of Floral Buds on the Growth of the Cotton Plant. *Annals of Botany* **23**, 636-649 (1959).
6. L. L. Hensel, M. A. Nelson, T. A. Richmond, A. B. Bleecker, The Fate of Inflorescence Meristems Is Controlled by Developing Fruits in Arabidopsis. *Plant Physiology* **106**, 863-876 (1994).
7. E. Burillo *et al.*, Seed production determines the entrance to dormancy of the inflorescence meristem of Pisum sativum and the end of the flowering period. *Physiol Plant* **176**, e14425 (2024).
8. K. C. Engvild, The death hormone hypothesis. *Physiologia Plantarum* **77**, 282-285 (1989).
9. M. O. Kelly, P. J. Davies, The Control of Whole Plant Senescence. *Crc Cr Rev Plant Sci* **7**, 139-173 (1988).
10. P. González-Suárez, C. H. Walker, T. Bennett, Bloom and bust: understanding the nature and regulation of the end of flowering. *Current Opinion in Plant Biology* **57**, 24-30 (2020).
11. C. H. Walker, T. Bennett, "Forbidden Fruit: Dominance Relationships and the Control of Shoot Architecture" in Annual Plant Reviews online, J. A. Roberts, Ed. (Wiley, 2018), pp. 217-254.
12. V. Balanzà, P. Merelo, C. Ferrándiz, Flowering also has to end: knowns and unknowns of reproductive arrest in monocarpic plants. *Journal of Experimental Botany* **74**, 3951-3960 (2023).
13. S. Shannon, D. R. Meekswagner, A Mutation in the Arabidopsis Tfl1 Gene Affects Inflorescence Meristem Development. *Plant Cell* **3**, 877-892 (1991).
14. M. Goetz, M. Rabinovich, H. M. Smith, The role of auxin and sugar signaling in dominance inhibition of inflorescence growth by fruit load. *Plant Physiology* **187**, 1189-1201 (2021).

15. C. H. Walker *et al.*, Cytokinin signaling regulates two-stage inflorescence arrest in Arabidopsis. *Plant Physiology* **191**, 479-495 (2023).
16. S. E. Wuest, M. A. Philipp, D. Guthörl, B. Schmid, U. Grossniklaus, Seed Production Affects Maternal Growth and Senescence in Arabidopsis. *Plant Physiology* **171**, 392-404 (2016).
17. Y. Wang *et al.*, Morphological and Physiological Framework Underlying Plant Longevity in Arabidopsis thaliana. *Front. Plant Sci.* **11**, 600726 (2020).
18. V. Balanzà *et al.*, Genetic control of meristem arrest and life span in Arabidopsis by a FRUITFULL-APETALA2 pathway. *Nat Commun* **9**, 565 (2018).
19. P. Merelo, I. González-Cuadra, C. Ferrándiz, A cellular analysis of meristem activity at the end of flowering points to cytokinin as a major regulator of proliferative arrest in Arabidopsis. *Current Biology* **32**, 749-762.e743 (2022).
20. I. Martínez-Fernández, S. Menezes De Moura, M. Alves-Ferreira, C. Ferrándiz, V. Balanzà, Identification of Players Controlling Meristem Arrest Downstream of the FRUITFULL-APETALA2 Pathway. *Plant Physiology* **184**, 945-959 (2020).
21. J. Kim *et al.*, New Clothes for the Jasmonic Acid Receptor COI1: Delayed Abscission, Meristem Arrest and Apical Dominance. *PLoS ONE* **8**, e60505 (2013).
22. V. Sanchez-Gerschon *et al.*, Transcription factors HB21/40/53 trigger inflorescence arrest through abscisic acid accumulation at the end of flowering. *Plant Physiol* **195**, 2743-2756 (2024).
23. A. Ware *et al.*, Auxin export from proximal fruits drives arrest in temporally competent inflorescences. *Nature Plants* **6**, 699-707 (2020).
24. I. Bartrina, E. Otto, M. Strnad, T. Werner, T. Schmülling, Cytokinin Regulates the Activity of Reproductive Meristems, Flower Organ Size, Ovule Formation, and Thus Seed Yield in Arabidopsis thaliana. *The Plant Cell* **23**, 69-80 (2011).
25. I. Bartrina *et al.*, Gain-of-Function Mutants of the Cytokinin Receptors AHK2 and AHK3 Regulate Plant Organ Size, Flowering Time and Plant Longevity. *Plant Physiology* **173**, 1783-1797 (2017).
26. T. Kuroha *et al.*, Functional Analyses of LONELY GUY Cytokinin-Activating Enzymes Reveal the Importance of the Direct Activation Pathway in Arabidopsis. *The Plant Cell* **21**, 3152-3169 (2009).
27. I. Schwarz *et al.*, Cytokinin regulates the activity of the inflorescence meristem and components of seed yield in oilseed rape. *Journal of Experimental Botany* **71**, 7146-7159 (2020).
28. S. P. Gordon, V. S. Chickarmane, C. Ohno, E. M. Meyerowitz, Multiple feedback loops through cytokinin signaling control stem cell number within the shoot meristem. *P Natl Acad Sci USA* **106**, 16529-16534 (2009).
29. C. Riou-Khamlichi, R. Huntley, A. Jacqmard, J. A. H. Murray, Cytokinin activation of cell division through a D-type cyclin. *Science* **283**, 1541-1544 (1999).
30. A. Osugi *et al.*, Systemic transport of trans-zeatin and its precursor have differing roles in Arabidopsis shoots. *Nature Plants* **3**, 17112 (2017).
31. Y. Hu, E. Shani, Cytokinin activity – transport and homeostasis at the whole plant, cell, and subcellular levels. *New Phytologist* **239**, 1603-1608 (2023).
32. P. E. Jameson, Cytokinin Translocation to, and Biosynthesis and Metabolism within, Cereal and Legume Seeds: Looking Back to Inform the Future. *Metabolites* **13**, 1076 (2023).
33. C. Wenzl, J. U. Lohmann, 3D imaging reveals apical stem cell responses to ambient temperature. *Cells & Development* **175**, 203850 (2023).
34. N. Prunet, T. P. Jack, E. M. Meyerowitz, Live confocal imaging of Arabidopsis flower buds. *Dev Biol* **419**, 114-120 (2016).
35. L. Willis *et al.*, Cell size and growth regulation in the Arabidopsis thaliana apical stem cell niche. *Proc Natl Acad Sci U S A* **113**, E8238-E8246 (2016).

36. S. Valuchova *et al.*, Imaging plant germline differentiation within Arabidopsis flowers by light sheet microscopy. *Elife* **9** (2020).
37. R. Yokoyama, T. Hirakawa, S. Hayashi, T. Sakamoto, S. Matsunaga, Dynamics of plant DNA replication based on PCNA visualization. *Sci Rep* **6**, 29657 (2016).
38. J. Craft *et al.*, New pOp/LhG4 vectors for stringent glucocorticoid-dependent transgene expression in Arabidopsis. *Plant J* **41**, 899-918 (2005).
39. S. Sharma, P. Kaur, K. Gaikwad, Role of cytokinins in seed development in pulses and oilseed crops: Current status and future perspective. *Front. Genet.* **13**, 940660 (2022).
40. G. C. Terceros *et al.*, The Importance of Cytokinins during Reproductive Development in Arabidopsis and Beyond. *IJMS* **21**, 8161 (2020).
41. D. Ko *et al.*, Arabidopsis ABCG14 is essential for the root-to-shoot translocation of cytokinin. *Proc. Natl. Acad. Sci. U.S.A.* **111**, 7150-7155 (2014).
42. K. Zhang *et al.*, Arabidopsis ABCG14 protein controls the acropetal translocation of root-synthesized cytokinins. *Nat Commun* **5**, 3274 (2014).
43. B. Landrein *et al.*, Nitrate modulates stem cell dynamics in Arabidopsis shoot meristems through cytokinins. *Proc. Natl. Acad. Sci. U.S.A.* **115**, 1382-1387 (2018).
44. R. Abualia *et al.*, Molecular framework integrating nitrate sensing in root and auxin-guided shoot adaptive responses. *Proc. Natl. Acad. Sci. U.S.A.* **119**, e2122460119 (2022).
45. H. Thomas, Senescence, ageing and death of the whole plant. *New Phytol* **197**, 696-711 (2013).
46. D. Volkava, K. Riha, Growing old while staying young : The unique mechanisms that defy aging in plants. *EMBO Rep* **25**, 934-938 (2024).
47. P. González-Suárez, C. H. Walker, T. Bennett, FLOWERING LOCUS T mediates photo-thermal timing of inflorescence meristem arrest in Arabidopsis thaliana. *Plant Physiology* **192**, 2276-2289 (2023).
48. R. Gutzat *et al.*, Arabidopsis shoot stem cells display dynamic transcription and DNA methylation patterns. *EMBO J* **39**, e103667 (2020).
49. G. Daum, A. Medzihradszky, T. Suzaki, J. U. Lohmann, A mechanistic framework for noncell autonomous stem cell induction in Arabidopsis. *Proc Natl Acad Sci U S A* **111**, 14619-14624 (2014).
50. J. Friml *et al.*, Efflux-dependent auxin gradients establish the apical-basal axis of Arabidopsis. *Nature* **426**, 147-153 (2003).
51. E. Zurcher *et al.*, A robust and sensitive synthetic sensor to monitor the transcriptional output of the cytokinin signaling network in planta. *Plant Physiol* **161**, 1066-1075 (2013).
52. M. Cerny *et al.*, Proteome and metabolome profiling of cytokinin action in Arabidopsis identifying both distinct and similar responses to cytokinin down- and up-regulation. *J Exp Bot* **64**, 4193-4206 (2013).
53. A. K. Wilson, F. B. Pickett, J. C. Turner, M. Estelle, A dominant mutation in Arabidopsis confers resistance to auxin, ethylene and abscisic acid. *Mol Gen Genet* **222**, 377-383 (1990).
54. S. Preibisch, S. Saalfeld, J. Schindelin, P. Tomancak, Software for bead-based registration of selective plane illumination microscopy data. *Nat Methods* **7**, 418-419 (2010).
55. S. el-Showk *et al.*, Parsimonious Model of Vascular Patterning Links Transverse Hormone Fluxes to Lateral Root Initiation: Auxin Leads the Way, while Cytokinin Levels Out. *PLOS Computational Biology* **11**, e1004450 (2015).

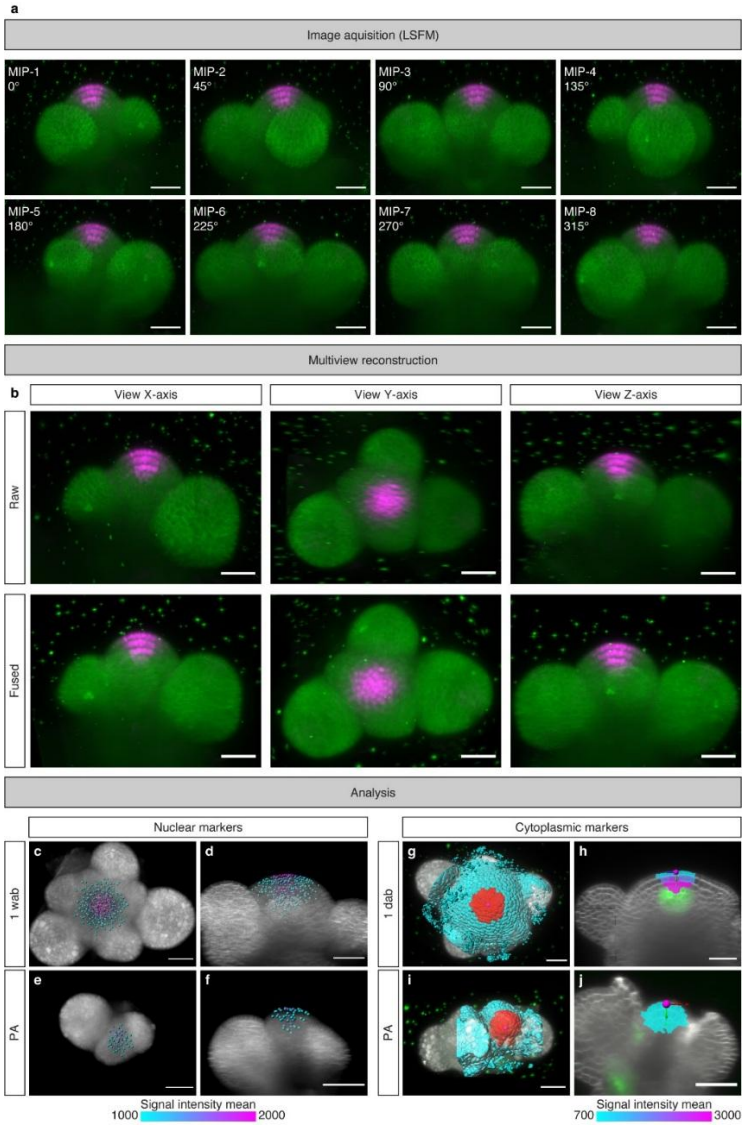

Fig. 1. Quantitative 3D imaging of Arabidopsis inflorescence meristem. (a) Maximum intensity projections (MIPs) of IM expressing *pCLV3::H2B-mCherry* (magenta) and the plasma membrane marker *SYP132:GFP* (green) scanned from eight different angles. Scale bar = 30 µm. (**b)** Comparison of image quality from a single angle stack (above) and all angles fused together (below) **(c-f)** 3D-reconstructions of IMs 1 wab (c,d) and at PA (e,f) with the segmented nuclear *pCLV3::H2B-mCherry* signal. Relative signal intensity means of the segmented nuclei are indicated by colormap. Plasma membrane is highlighted by *SYP132:GFP* (gray). (c,e) represent top views and (d,f) longitudinal sections, respectively. Scale bar = 30 µm. **(g-j)** 3D-reconstructions of IMs 1 wab (g,h) and at PA (i,j) with cells segmented using plasma membrane signal obtained by FM4-64 staining (gray). (g,i), Top views of surface rendered models. Red color indicates cells within 21 µm from meristem apex that were used for quantitative analysis of cytoplasmic signal. (h,i) Longitudinal sections of the segmented IMs. Intensity means of the *TCSn::GFP* signal in cells within 21 µm from the apex are indicated by heatmaps. *TCSn::GFP* signal outside of that volume is displayed in green. A reference frame (magenta sphere with arrows) indicates position of the meristem apex. Scale bar = 30 µm.

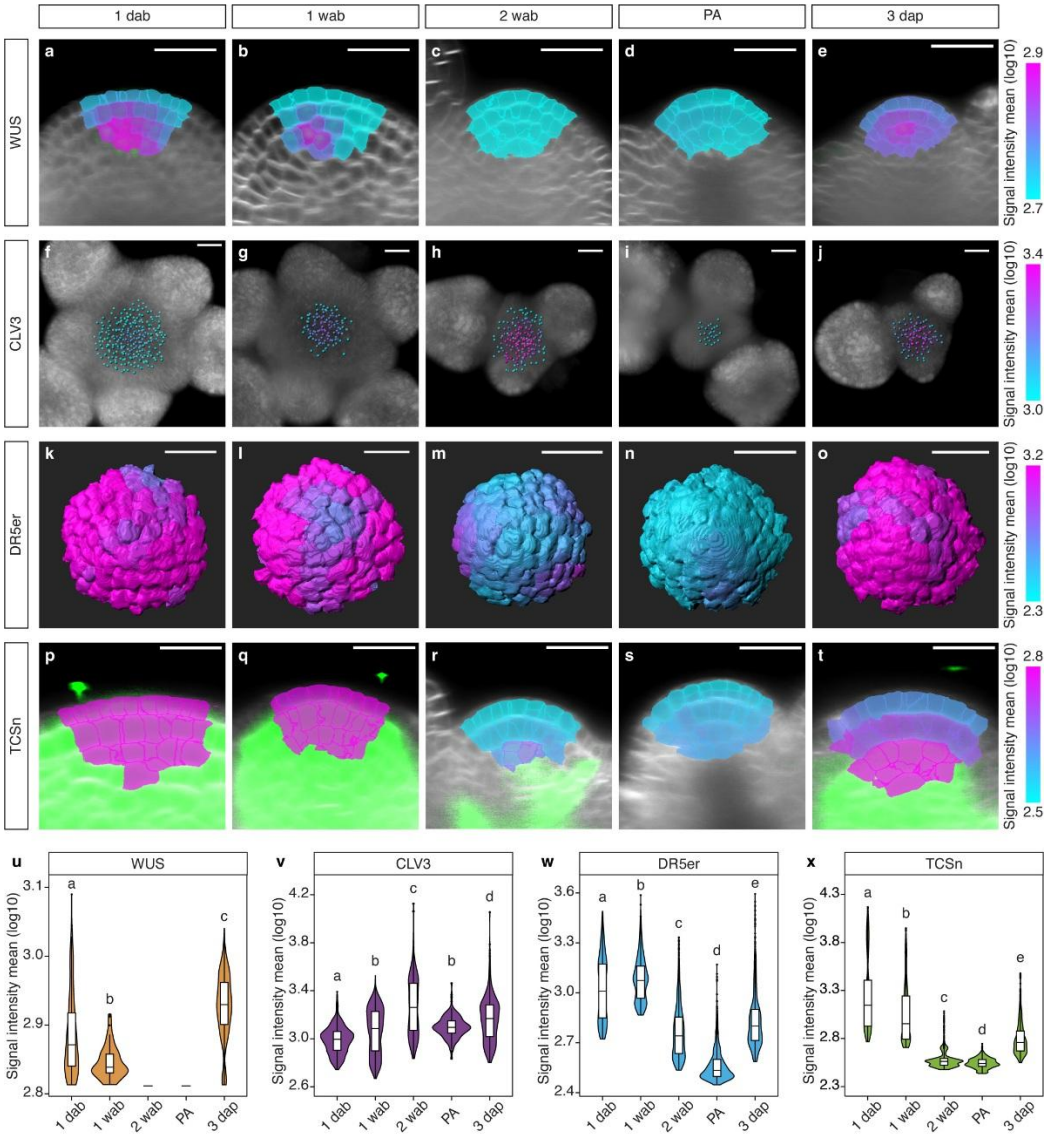

Fig. 2. Age-dependent changes in inflorescence meristems. (a-e) Top views of 3D IM reconstructions with segmented *pCLV3::H2B-mCherry* nuclei. Mean intensity of the signal is shown by colormap. Plasma membrane is highlighted by *SYP132:GFP* (gray). **(f-j)** Longitudinal sections through IM models; colormap indicates mean intensity of the *pWUS::WUS-linker-GFP* signal in cells within 21 µm form the meristem apex . Plasma membrane is stained with FM4-64. **(k-o)** Longitudinal sections through IM models; colormap indicates mean intensity of *TCSn::GFP* signal in cells within 21 µm form the meristem apex. Green indicates *TCSn::GFP* signal outside the analyzed volume. Plasma membrane is stained with FM4-64. **(p-t)** Top views of segmented cells in 3D IM models that are within 21 µm form the meristem apex. Heatmaps indicate mean intensity of the *DR5rev::GFP* signal in each cell. Scale bars = 20 µm. **(u-x)** Quantification of mean signal intensity of *pCLV3::H2B-mCherry* (u), *pWUS::WUS-linker-GFP* (v), *TCSn::GFP* (w) and *DR5rev::GFP* (x) in IMs at 1 dab, 1 wab, 2 wab, PA and 3 days after pruning (dap) is shown by hybrid violin-box plots. In (v), a cutoff of 2.8 was applied to exclude the background signal. Charts with different lowercase letters are significantly different from each other (ANOVA, Tukey's HSD test; p-value < 0.01, 215-1040 cells from 5 different meristems were included for each category).

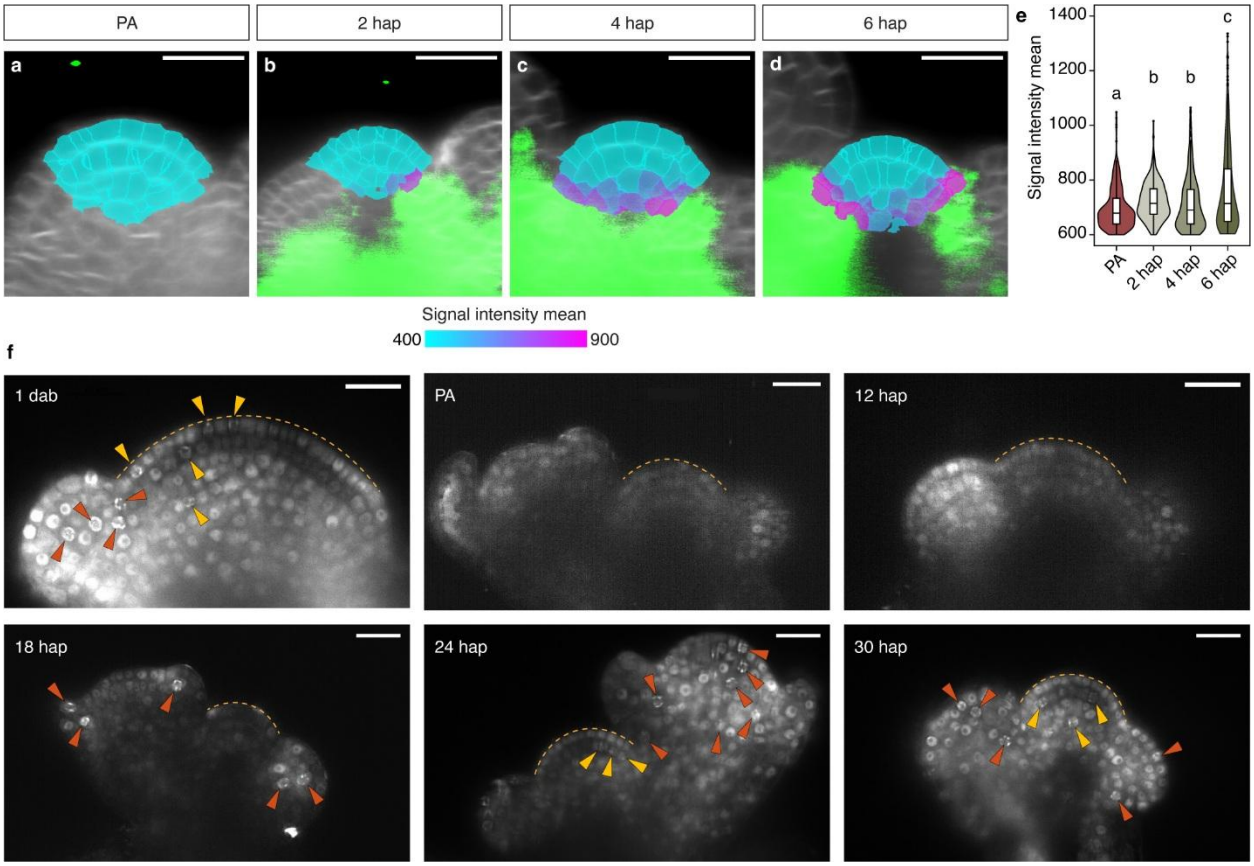

Fig. 3. Reactivation of inflorescence meristem by pruning. (a-d) Longitudinal sections of IM reconstructions showing *TCSn::GFP* expression at PA (a), 2 hours after pruning (hap) (b), 4 hap (c) and 6 hap (d). Segmented cells within 21 µm form the meristem apex were color-coded according to heatmaps, indicating signal intensity mean. Cell membranes (gray) were highlighted using FM4-64. Scale bars = 20 µm. **(e)** Quantification of mean signal intensity of *TCSn::GFP* in samples as in (a–d) shown by hybrid violin-box plots. To exclude the background signal, an intensity cutoff of 600 was applied. Charts with different lowercase letters are significantly different from each other (ANOVA, Tukey's HSD test; p-value < 0.01, 857-917 cells from 5 different meristems were included for each category). **(f)** Micrographs showing longitudinal sections of IMs with *PCNA:TagRFP* expression (gray). Inflorescences were imaged at 1 dab, PA, 12 hap, 18 hap, 24 hap and 30 hap and shown micrographs represented representatives from at least five IMs for each stage. A yellow dashed line outlines the IM dome. Arrowheads point to nuclei in S-phase located in inflorescence meristem (yellow) and flower primordia from stage P2 (orange). Scale bars = 20 µm.

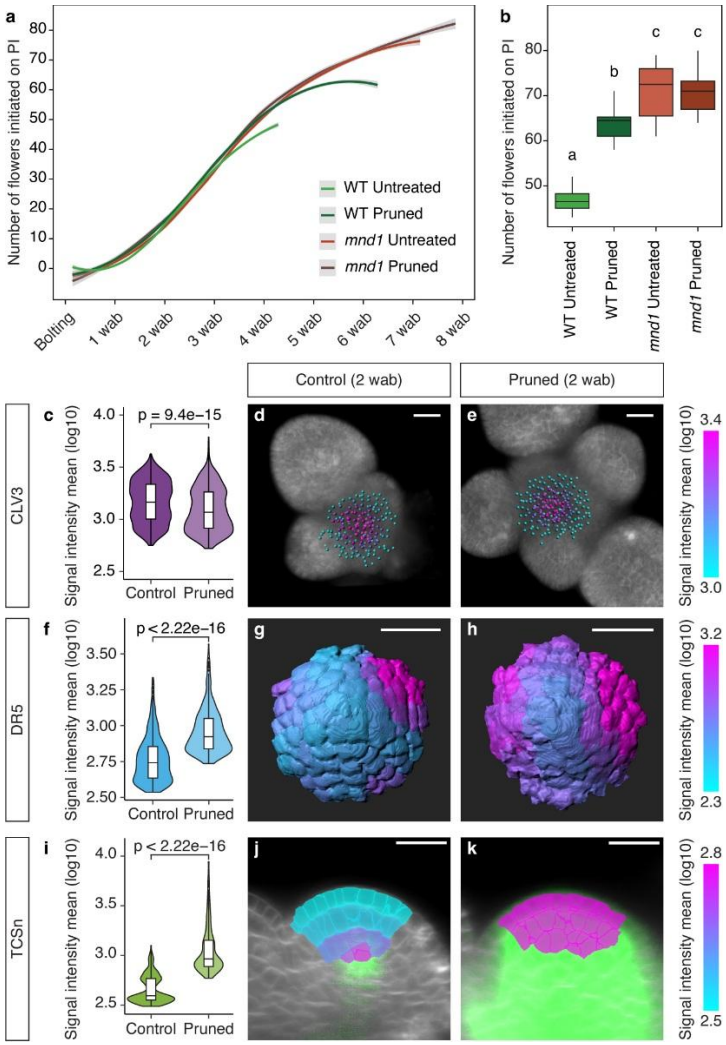

Fig. 4. Effect of fruits on inflorescence meristem. (a) Trend lines showing the number of flowers initiated on PI in untreated and continuously pruned wild type and sterile *mnd1* mutants, respectively. Trend lines are calculated using the loess fitting method; grey areas represent confidence intervals of 0.95. n = 20 plants per treatment. **(b)** Box plot showing total number of flowers initiated on PI of samples as in (a). Box plots with different lowercase letters are significantly different from each other (ANOVA, Tukey HSD test; p-value < 0.01). **(c-e)** *pCLV3::H2B-mCherry* signal quantification in IM of pruned and untreated WT plants. (d,e) Top views of 3D IM reconstructions with segmented *pCLV3::H2B-mCherry* nuclei. Mean intensity of the signal is shown by heatmap. Plasma membrane is highlighted by *SYP132:GFP* (gray). **(f-h)** *DR5rev::GFP* signal quantification in IM of pruned and untreated WT plants. (g,h) Top views of segmented cells that are within 21 µm form the meristem apex. Heatmap indicates mean intensity of the *DR5rev::GFP* signal in each cell. **(i-k)** *TCSn::GFP* signal quantification in IM of pruned and untreated WT plants. Longitudinal sections through IM models; heatmap indicates mean intensity of *TCSn::GFP* signal in cells within 21 µm form the meristem apex. Green indicates *TCSn::GFP* signal outside the analyzed volume. Plasma membrane stained with FM4-64 is indicated in gray. Scale bars = 20 µm. Hybrid violin-box plots indicate quantification of signal intensity mean of *pCLV3::H2B-mCherry* (c), *DR5rev::GFP* (f) and *TCSn::GFP* (i) (714-919 cells from 5 different meristems were included for each category). The statistical significance of differences between pruned and untreated plants was calculated using the Wilcoxon signed-rank test.

581

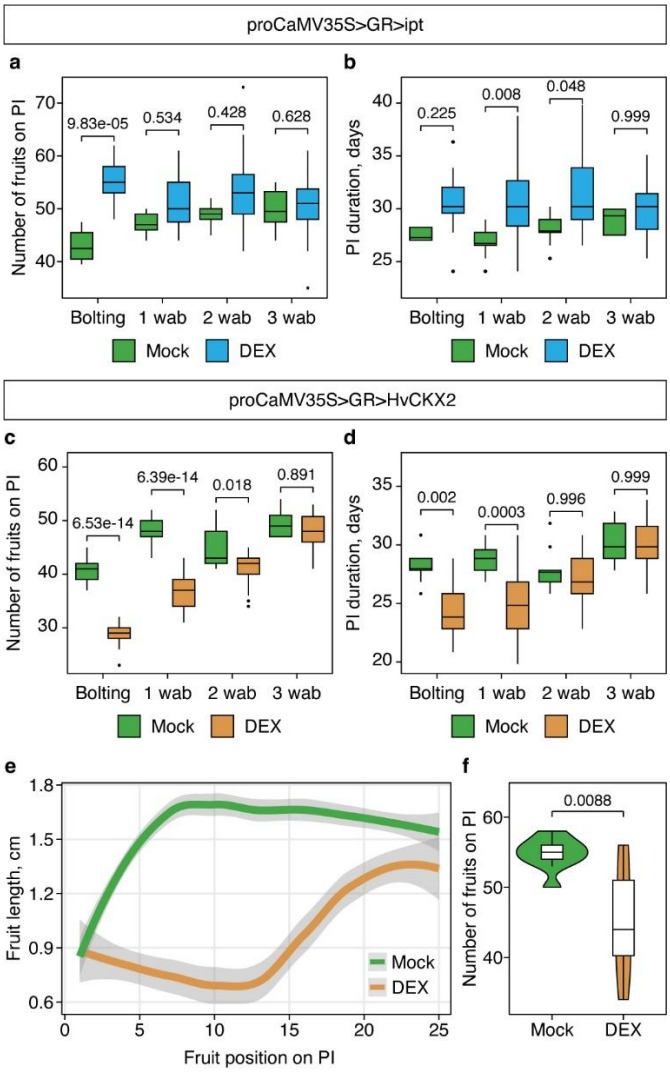

582
583
584

585 **Fig. 5. Effect of cytokinin levels on PA. (a,b)** Box plots showing effect of *proCaMV35S>GR>ipt* induction
586 on number of fruits on PI (a) and PI duration (b) after treating plants at bolting, 1, 2 and 3 wab either with
587 mock (n = 9, 9, 9 and 8 plants, respectively), or with DEX (n = 15, 23, 23 and 22 plants, respectively). **(c,d)**
588 Box plots showing effect of *proCaMV35S>GR>HvCKX2* induction on number of fruits on PI (a) and PI
589 duration (b) after treating plants at bolting, 1, 2 or 3 wab either with mock (n = 10, 9, 9 and 10 plants,
590 respectively), or with DEX (n = 17, 21, 21 and 22 plants, respectively). **(e)** Trend lines showing the length
591 of fruits formed on PI as indicative of fertility of proCaMV35S>GR>HvCKX2 plants after local treatment
592 with mock (n=11 plants) or DEX (n=10 plants). Trend lines are calculated using the loess fitting method;
593 grey areas represent confidence intervals of 0.95. **(f)** Violin-box plots showing effect of
594 proCaMV35S>GR>HvCKX2 induction on number of fruits on PI in the same plants as in (e). Statistical
595 significance of differences between the group means in (a-d, f) was calculated using the Wilcoxon signed-
596 rank test.
597

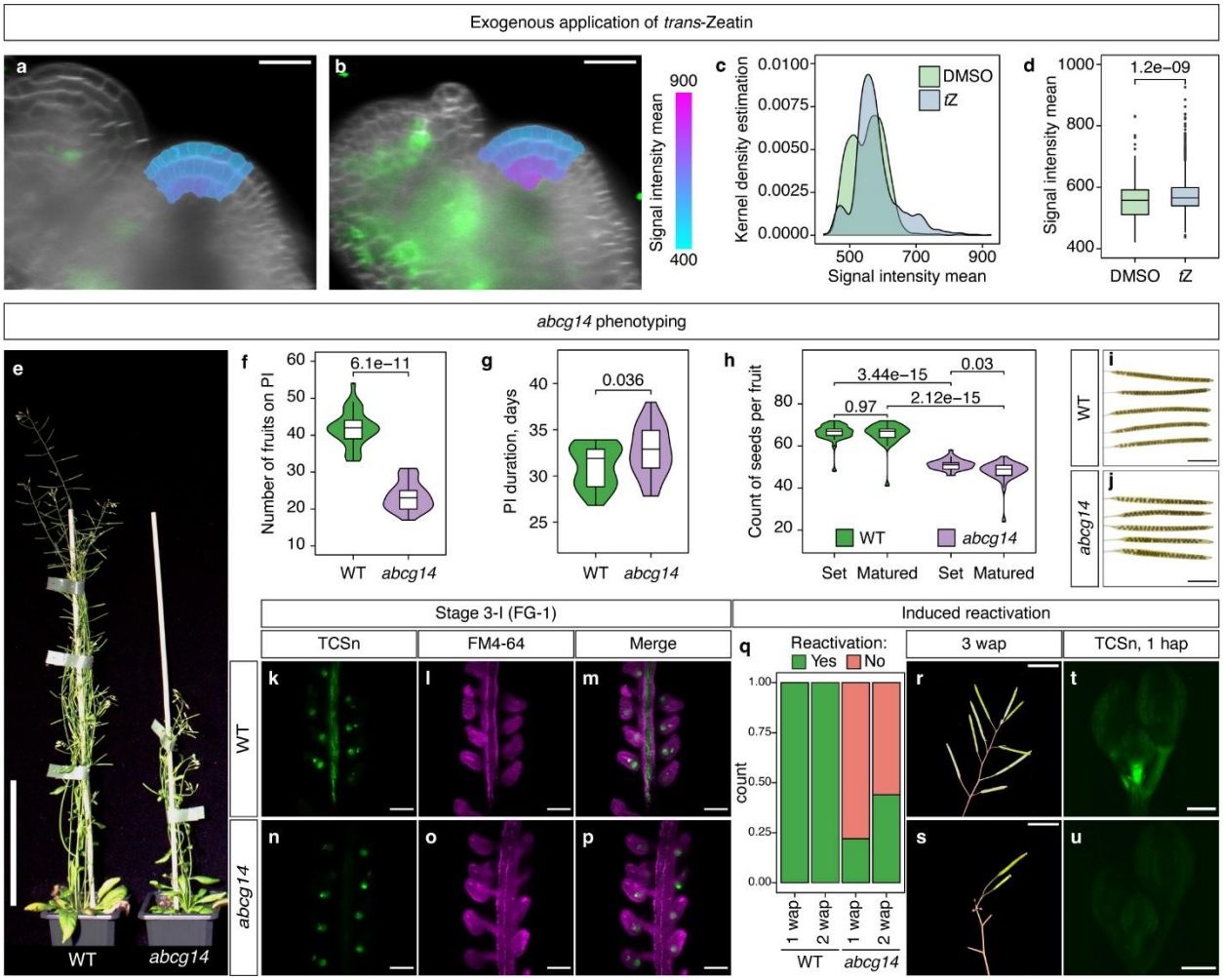

Fig. 6. Effect of cytokinin transport on PA. (a,b) Longitudinal sections of IMs expressing *TCSn::GFP* (green) from inflorescences treated at PA by application of DMSO (a) or 300 µM *trans*-Zeatin (b) in lanolin paste. The lanoline paste was applied to the inflorescence stem internode separated by 20 fruits from unopened buds and meristems were imaged 48 hours after treatment. Heatmap indicates mean intensity of the *TCSn::GFP* signal in cells within 21 µm form the meristem apex. Plasma membrane stained with FM4-64 is indicated in gray. Scale bars = 20 µm. **(c,d)** Quantification of mean signal intensity of *TCSn::GFP* in IMs of *t*Z treated inflorescences shown in kernel density (c) and box plots (d). The statistical significance of differences between the mean of groups was calculated using the Wilcoxon signed-rank test (n = 828 and 858 cells combined from five different meristems for DMSO and *t*Z treated samples, respectively). **(e)** Representative picture of 45-days-old wild type (Col-4) and *abcg14* plants. Scale bar = 10 cm. **(f,g)** Violin-box plots showing the number of fruits on PI (f) and PI duration (g) in wild type and *abcg14*. The statistical significance of differences between the mean of groups was calculated using the Wilcoxon signed-rank test (n = 29 plants for each genotype). **(h)** Violin-box plot showing set of ovules and matured seeds per fruit in wild type and *abcg14*. The statistical significance of differences between mean of groups was calculated using the Wilcoxon signed-rank test (n = 30 fruits at position 5-10 on PI from total from 5 different PIs). **(i,j)** Images of cleared mature fruits from the same position on PI of wild type (m) and *abcg14* (n). Scale bar = 5 mm. **(k-p)** Micrographs showing MIPs of pistils from wild type and *abcg14* plants expressing *TCSn::GFP* (green). Pistils were imaged with ovules at stage FG-1 (k–m) and with embryos at the pre-globular stage (n–p). Cell membranes (magenta) were highlighted using FM4-64. Scale bar = 100

619 μm. **(q-s)** Reactivation of IM in *abcg14* plants. (q) Bar charts showing fraction count of induced reactivation
620 of PIs in wild type and *abcg14* plants (n = 50 plants per group). (r,s) Representative pictures showing
621 reactivated meristems in wild type (r) and *abcg14* mutant (s). Scale bar = 5 mm. (t,u) Micrographs showing
622 MIPs of inflorescences at 1 hour after pruning from wild type and *abcg14* plants expressing *TCSn::GFP*
623 (green). Scale bar = 300 um.
624

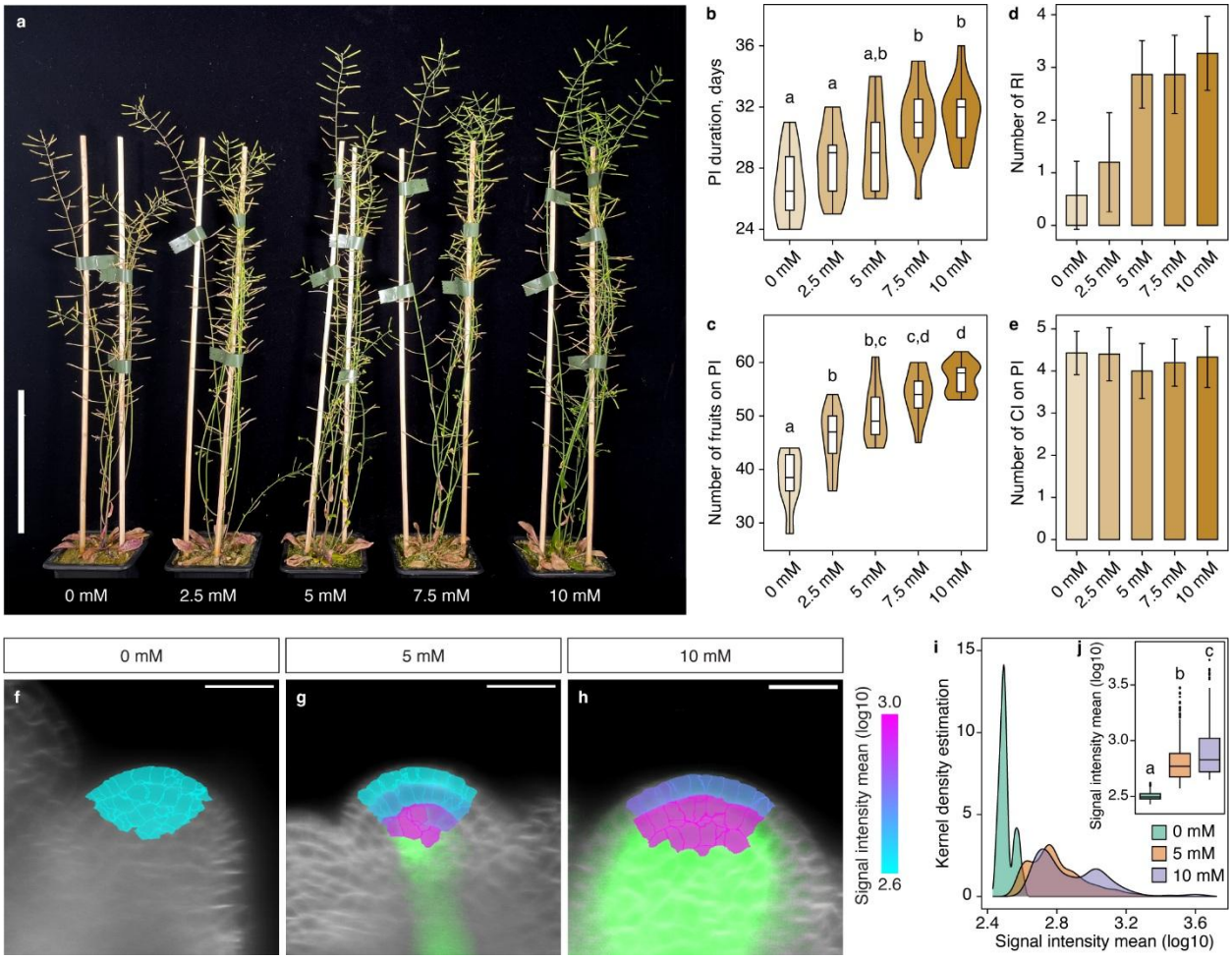

Fig. 7. Effect of nitrate levels on meristem arrest. (a) A representative picture of plants grown on substrate supplemented with different KNO3 concentrations. The picture was taken when plants of all treatment groups reached PA. Scale bar = 10 cm. (**b,c)** Violin-box plots showing PI duration (b) and number of fruits on PI (c) in plants grown on different KNO3 concentrations. Plots with different lowercase letters are significantly different from each other (ANOVA, Tukey HSD test; p-value < 0.01, n = 15 plants per treatment). **(d,e)** Bar charts showing mean number of rosette inflorescences (RI) (d) and cauline inflorescences (CI) on PI (e) in plants of treatment groups as in (a). Error bars represent standard deviation (n = 15 plants per treatment). **(f-h)** Longitudinal sections of IMs expressing *TCSn::GFP* (green) from plants grown on different concentrations of KNO3 and imaged 2 wab. Heatmap indicates mean intensity of the *TCSn::GFP* signal in cells within 21 µm form the meristem apex. Plasma membrane stained with FM4-64 is indicated in gray. Scale bars = 20 µm. **(i-j)** Quantification of the mean signal intensity of *TCSn::GFP* in IMs from plats grown at different concentrations of KNO3 shown in kernel density and box plots (inset). Plots with different lowercase letters are significantly different from each other (ANOVA, Tukey HSD test; p-value < 0.01; n = 877, 784 and 808 cells combined from five different meristems from plants grown at 0 mM, 5 mM and 10 mM KNO3, respectively).

644 **Movie 1. 3D reconstruction of the Arabidopsis inflorescence meristem expressing *pCLV3::H2B-mCherry***
645 **2 wab**. Nuclei expressing *pCLV3::H2B-mCherry* are indicated in red, the plasma membrane is visualized
646 with *SYP132:GFP* (green).
647
648 **Movie 2. 3D reconstruction of the Arabidopsis inflorescence meristem expressing *TCSn::GFP* 1 dab**. The
649 *TCSn::GFP* is indicated in red, the plasma membrane is visualized by FM4-64 staining (gray). The animation
650 also shows segmented cells that were within 21 µm of the meristem apex.
651
652
653